The effect of duct size, sample size, and fuel composition on concurrent flame spread over large cellulose samples in microgravity

Sandra L. Olson, Gary A. Ruff, Paul V. Ferkul, Jay C. Owens, John Easton, Ya-Ting Liao, James S. T'ien, Balazs Toth, Grunde Jomaas, Carlos Fernandez-Pello, Guillaume Legros, Augustin Guibaud, Osamu Fujita, Nikolay Smirnov, David L. Urban

Abstract

Concurrent flame spread data for thermally-thin charring solid fuels are presented from Saffire and BASS experiments performed in habitable spacecraft for three duct sizes, five sample sizes, two materials, and two atmospheres. The flame spread rates and flame lengths were strongly affected by duct size even for the relatively large ducts (> 30 cm tall). A transient excess pyrolysis length (i.e., flame length overshoot) was observed for the cotton fabric that burned away, which indicates that the transient excess pyrolysis length phenomenon is caused by more than just the flame moving into the developing boundary layer thickness as was the case with the SIBAL sample. A burnout time, defined as the pyrolysis length divided by the flame spread rate, normalized the pyrolysis length histories into a single curve with a steady burnout time of 22 s for the SIBAL fabric. The transient excess pyrolysis length is hypothesized to be a post-ignition flame growth transient for the essentially two-dimensional flames where the burnout time becomes very long until the preheat and pyrolysis lengths develop. The three-dimensional flames over narrow samples have lateral thermal expansion and lateral oxygen diffusion which allows them to transition to a steady state length without the transient excess pyrolysis length. Surface temperature profiles, nondimensionalized by the pyrolysis length, indicate that the temperature profiles exhibit the same shape across the pyrolysis zone. A surface energy balance calculation in the preheat region revealed that the heat flux increased rapidly at the pyrolysis front to near the critical heat flux for ignition. An estimate of the acceleration of the inviscid core flow in the duct due to thermal expansion and developing boundary layers on the duct walls and the SIBAL sample surface seems to explain the observed spread rate trends across three duct sizes and multiple sample sizes.

Keywords: concurrent flame spread, microgravity, duct size, sample size, cellulose fabrics

Nomenclature

A	= area, cm^2
A_s	= preexponential factor, s^{-1}
$C_{p,f}$	= specific heat of the fuel vapor, J/g K
C_s	= specific heat of the solid, J/g K
E_s	= activation energy, J/mol
f'	$=U/U_\infty$
H	= height, cm
k	= thermal conductivity, W/cm K
ℓ	= sample length, cm
L	= length, cm
L_v	= latent heat of vaporization, J/g
P	= pressure, kPa

$\dot{q}_f''$ = heat flux from the flame to the surface of the fuel per side, W/cm^2 s

R = ideal gas constant, 8.3145 J/mol K

SIBAL = Solid Inflammability Boundary At Low-speed, cotton-fiberglass blend fuel

t = time, s

T = temperature, ^{o}C or K

U = velocity, cm/s

V_f = flame spread rate, cm/s

V = volume, cm^3

w = sample width, cm

W = duct width, cm

x = distance along the sample in the flow direction, starting at the ignition end, cm

y = distance perpendicular to the sample, cm

Greek

δ = boundary layer thickness, cm

δ* = displacement thickness, cm

ε = emissivity

η = Blasius boundary layer non-dimensional thickness, Eq. (8)

ρ = density, g/cm^3

σ = Stefan-Boltzmann constant, 5.67 $\times 10^{-8}$ W·m^{-2}·K^{-4}

τ = thickness, cm

υ = kinematic viscosity, cm^2/s

Subscripts and Superscripts

BL = boundary layer

duct = duct

f = flame

holder = holder

∞ = ambient

mean = mean

p = pyrolysis

s = solid

ss = steady state

1. Introduction

As humans press ever outward into space, so too do they take with them the risk of fire in their spacecraft. The series of Saffire experiments aboard the habitable, but unmanned, Cygnus spacecraft are investigating meter-scale fires in space and the impact they have on the spacecraft. The results from Saffire I-III have been reported [1-3] and an overview of flights IV and V has also been published [4], so the focus here is on results related to concurrent flame spread over SIBAL (a cotton-fiberglass blend) and pure cotton fabric samples extracted from flights IV and V, respectively. Comparisons are made to the previous SIBAL fuel flight data as well. New variables that are studied in Saffire IV and V include a change in the duct height, material differences (SIBAL fabric versus cotton knit and sample length), and normoxic oxygen and pressure conditions.

Concurrent flame spread in microgravity has been the subject of considerable research in the last few decades. Markstein and de Ris first showed that upward flame spread could result in a constant flame size for large samples [5]. Normal gravity [6] and drop tower experiments [7, 8] showed that much could be learned about concurrent flame spread from simple experiments.

Ever increasingly complex models included surface [9] and gas-phase radiation [10], two-dimensional steady [11] to three-dimensional transient [12]. The effect of duct confinement was evaluated for single samples [13] and arrays of samples [14,15]. Concurrent flame spread for thin fuels was shown to have a limiting length [16]. The three-dimensional transient model predictions have been compared with the previous Saffire experiments [17]. A two-dimensional model was used to evaluate the effects of forced flow, ambient oxygen concentration and pressure on concurrent flame spread over wide samples. Scaling analyses [8, 23-26] showed the relevant non-dimensional parameters included Grashof, Reynolds, Planck, and Nusselt numbers.

The size of the flow duct has recently been revealed to play a significant role in the concurrent flame spread as supported by models [13-15, 19-22]. Shih and T'ien [13] showed with their three-dimensional steady model that the duct size affected the flame spread rate. At higher velocity, the spread rate decreased for small duct widths (i.e., narrow channels). At low velocities, lateral oxygen diffusion becomes a significant factor by increasing the flame spread rate even for small duct widths. Shih and Wu [15] conducted multiple parallel sheet experiments in normal gravity and Shih [14] used a two-dimensional model to evaluate concurrent flame interactions as spacing between samples was reduced from 150 mm (experiments) and 500 mm (model) down to quenching at a few centimeters. Non-monotonic flame spread rates have been observed, with spread rates initially increasing as the channel height is reduced because of flow acceleration due to thermal expansion and enhanced heat transfer from radiant exchange. However, at smaller channel heights, the flame spread rate decreases because the oxygen is consumed at the flame base and does not penetrate the channel. Although the steady model failed to converge to a steady state at some duct heights, there appears to be a maximum spread rate at intermediate channel heights that was confirmed with the experiments. Li and co-workers [19-22] conducted ISS experiments on concurrent flame spread in various duct sizes and used a three-dimensional transient model to compare to the experiments. The model showed that the flame spread rate was non-monotonic with duct size, as observed by the experiments. As the size was reduced, the flame spread rate increased because of thermal expansion. However, upon further reduction, the flame spread rate slowed due to limited oxygen supply and heat loss to the encroaching walls. The amount of oxygen available is controlled by the upstream fan in microgravity unlike in normal gravity where the flame can entrain increasing amounts of oxygen as it grows. Saffire IV is a repeat of the test conditions from Saffire I with a smaller duct and will thus test our current understanding of the effect of duct size on concurrent flame spread.

Sample size effects on upward or concurrent flame spread have been studied over a wide range of sample sizes. Markstein and de Ris [5] were the first to show steady upward flame spread over very large samples (up to 91.4 cm wide). Honda and Ronney [23] varied the sample width from 4 mm to 100 mm and showed via scaling that for samples less than approximately 10 mm wide, the spread rate varies with the cube of the width and are convectively stabilized. Above approximately 10 mm wide, the spread rate varies as the square root of the width and was stabilized by radiation. Experiments have shown that upward flame spread can reach a steady size in normal gravity at reduced pressure [6, 24, 27]. Li et al. [17] numerically modeled the Saffire I and II experiments, which had different sample widths. The model predicted the observed transient excess pyrolysis length (overshoot) seen for the wide samples, which they

attributed to the growing boundary layer as the flame spread downstream. The model also predicted the observed lack of a transient excess pyrolysis length for the narrow samples since the samples were deep within the flow boundary layer where they were positioned half-way down the duct. Saffire V, which used a cotton fabric with the same total area density as the SIBAL fabric, will further test the boundary layer hypothesis as the cause of the transient excess pyrolysis length since the material burns away completely, so the flame base is exposed to the free stream velocity.

Research into the effects of ambient oxygen concentration and pressure effects on concurrent flames has also been conducted [6, 18, 24, 25, 28]. The experimental studies have shown that the Grashof scaling P^2g closely correlated upward flame spread [25]. Other experiments have found that the concurrent flame spread rate varies linearly with flow rate (over the range tested) and oxygen concentration but with the square root of pressure via convective heat transfer scaling [8, 24]. Early two-dimensional models predicted the flame spread rate varied linearly with flow velocity and oxygen concentration [9], but a recent three-dimensional model [18] indicated that the spread rate varies linearly with pressure and flow but as the square of the oxygen concentration. Most recently, Zhao et al. [29] correlated upward flame spread rates over narrow samples with power laws of pressure at 5 different oxygen concentrations.

The objectives of this paper are to describe the results of Saffire IV and V and put them in perspective relative to the previous experiments. In the following, the experimental setup is described, and then the tracking of the flame spread rate and flame and pyrolysis lengths from the flame images are presented. Surface temperature data are analyzed, and those data are used to evaluate a surface energy balance in the preheat region. Lastly, the effect of duct size on the local flow is estimated based on thermal expansion and core flow acceleration due to boundary layer growth in the entrance region to the duct.

2. Experimental Setup

The large Saffire flow duct provides an oxidizer flow past the fuel samples. A cutaway of the duct is shown in Fig. 1a. The oxidizer is drawn in from the ambient air in the Cygnus vehicle and goes through a flow straightener before entering the duct. The flow uniformity was verified with smoke wire flow visualization during the flights. The flow exits in the positive x-direction back into the vehicle through another flow straightener. The exhaust follows a torturous path through the vehicle between the refuse bags and other discarded equipment before returning to the entrance to the duct. This is expected to provide uniform mixing in the large spacecraft volume, and the oxygen concentration can therefore be assumed to be constant for the duration of the test (approximately three minutes).

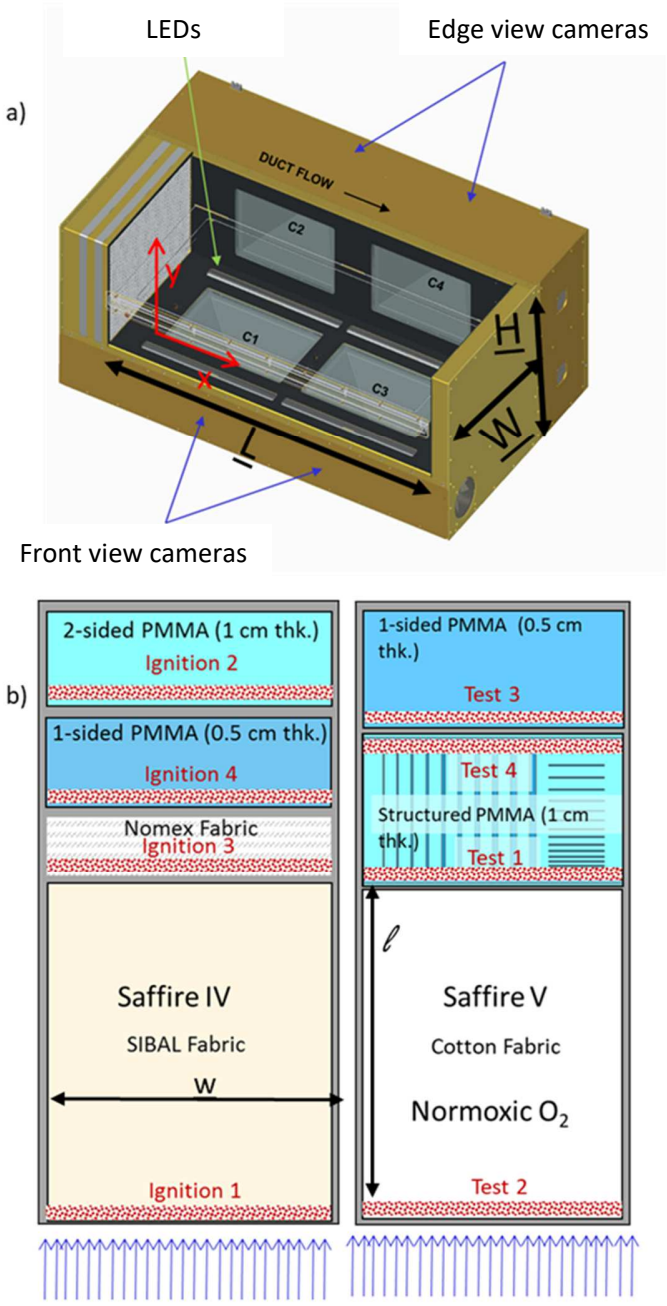

Figure 1: a) flow duct layout and dimensions L, W, and H are given in Table 1; b) sample card layouts for Saffire IV (left) and Saffire V (right) with sample dimensions w and l *are* given in Table 1.

Saffire IV and V added new side view cameras (C2 and C4 in Fig. 1a) that were not present for the prior flights. To fit these into the same volume of hardware, the duct height H had to be reduced from 51 cm to 30.5 cm. The sample card (shown as a transparent outline in the duct in Fig. 1a) is mounted along the centerline of the duct height and spans the full length, L, and width, W, of the duct. The sample card layouts for Saffire IV and V are shown in Figure 1b. In Saffire IV, the SIBAL fabric was positioned at the upstream edge of the sample card, and in Saffire V, the cotton fabric was positioned there. Cameras C1 and C2 are used to image these samples. These samples were the first samples to burn in each flight. The downstream samples [4] are not discussed here.

Both the SIBAL and the cotton fabric samples were w=40.6 cm wide and ℓ=50 cm long. Figure 2 shows closeups of the cellulosic materials burned in Saffire. The bleached organic interlock cotton fabric shown in Fig. 2a has an area density of 18.1 mg/cm^2. It was chosen to most closely match the total area density of SIBAL fabric. The SIBAL fabric shown in Fig. 2b is 75% unbleached cotton, 25% fiberglass, and has a total area density of 18.05 mg/cm^2 (13.54 mg/cm^2 cotton).

The samples are ignited on both sides of their upstream end with a sawtooth Kanthal A-1 © 29 gauge hot wire. Each igniter 'tooth' is 2.5 cm wide, and there are 16 teeth across each sample with each tooth alternating front/back. The igniter is energized for 8 s at 3.8 amps after the flow was established through the duct. The total ignition energy across the sample was 183 W.

The SIBAL fuel fabric is a custom-made blend. Each strand of the fabric is a mixture of the cotton and fiberglass. The cotton is mostly consumed during flame spread, leaving behind residual fuel smolder spots within the fiberglass matrix after the flame passage. The post burn fiberglass matrix is shown in Fig. 2c. The SIBAL fuel also proved to be easier to handle than cotton fabric in terms of sample preparation. The rigidity of SIBAL fabric made the fabric structurally more robust and less prone to stretching. The cotton fabric stretches up to 40% in the sample width direction but much less in the flame spread direction.

Both surface and edge view cameras were Allied Vision © (AVT) Manta G-235c GigE cameras with a Bayer Color Sensor recording at 30 frames per second with an auto exposure time of up to 0.03 s (the inverse of the framing rate). The gain was allowed to vary as the flame developed to best capture the flame as it grew but did not begin to vary until the maximum exposure time was reached. Green LED strips (shown in Fig. 1) blinked on for 3 frames every 2 seconds to illuminate the pyrolysis front while the dark images were used to measure the flame size and shape.

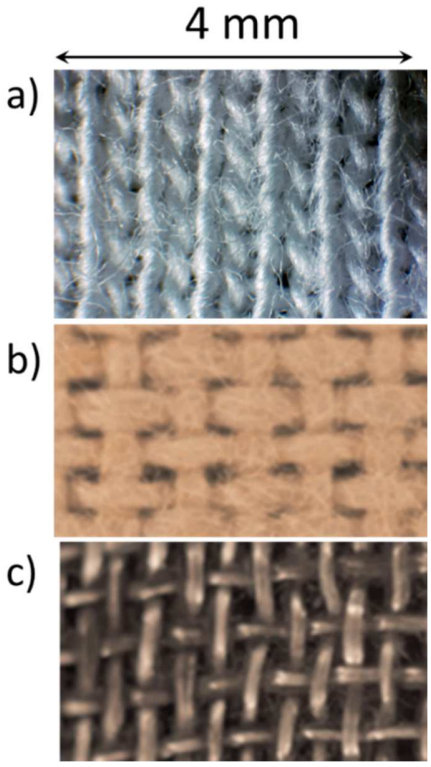

Figure 2: a) cotton Teloi© fabric; b) SIBAL fabric; c) fiberglass matrix exposed after material burned (from a ground test). The flame spread direction is vertical for all these images.

Both surface and edge view images were downlinked in highly compressed .jpg for operational purposes, and subsequently large RAW files were downlinked and converted to lossless .tiff formats for later scientific analysis. These images were distortion-corrected to remove the distortion caused by the large field of view and short working distance of the lens. The flame tracking was performed using the distortion-corrected tiff images since they were of the highest quality. The distortion-corrected tiffs for the surface view were a 1638 x 1325 pixels array while the .tiffs for the edge view were a 1982 x 609 pixels array to capture the full sample corresponding to 3.2 mm/pixel. The LED-illuminated surface view provided the pyrolysis front propagation information, and the dark images were enhanced to show the flame as displayed in Figs. 3, 4, and 5. The gain varied from 40 to a minimum of 32 (Saffire IV) and 24 (Saffire V).

The test matrix for the cellulosic samples in Saffire I-V and two BASS [30] tests is given in Table 1. Thermocouples were woven into the centerline of the samples with surface thermocouple locations starting from the upstream end noted in Table 1.

Table 1: Thin Fuel Concurrent Flow Test Matrix and Flame Measurements

Flight #	Sample #	Flow, cm/s	Sample dimensions ℓ x w, cm	Duct dimensions L x W x H, cm	O_2,+ % by vol	P, kPa	V_f, cm/s	L_f, cm	L_p, cm	H_f, cm	Surface TC locations, cm
I	1	20	SIBAL: 94 x 40.6 Holder: 109 x 46	109 x 46 x 51	21.7	102	0.18	4	4	2.0*	30, 60
II	5	20	SIBAL: 29 x 5 Holder: 109 x 46	109 x 46 x 51	22.1	103	0.21	4	4	1.0*	7.5
II	6	25	SIBAL: 29 x 5 Holder:109 x 46	109 x 46 x 51	22.1	103	0.26	5	5	0.9*	7.5
III	1	25	SIBAL: 94 x 40.6 Holder:109 x 46	109 x 46 x 51	21.2	99	0.23	5	5	1.8*	30, 60
IV	4	20	SIBAL: 50 x 40.6 Holder:109 x 46	109 x 46 x 30.5	23.1	99	0.36	8.5	8.5	2.7	30, 42
V	5	20	Cotton: 50 x 40.6 Holder:109 x 6	109 x 46 x 30.5	27.7	76	0.34	14	10	3.5	30, 42
BASS	11	19	SIBAL: 10 x 1.2 Holder: 13 x 2.7	17 x 7.6 x 7.6	21.5	101	0.27	2.2	n/a	0.4	n/a
BASS	4	22	SIBAL: 10 x 2.2 Holder: 13 x 3.8	17 x 7.6 x 7.6	21.6	101	0.51	6.2	n/a	0.6	n/a

+ The Cygnus vehicle was originally filled with the ISS atmosphere, which at hatch closing was recorded as listed in Table 1 for Saffire I-IV. In Saffire V, the vehicle was depressurized, and supplemental oxygen was added from an oxygen bottle so the near-normoxic test atmosphere was 27.7% O_2 at 76 kPa.

*Values are estimated since no side view was recorded. These values are only used in section 5.0 to estimate the flame thermal expansion effect on the flow.

3. Results

The primary data comes from the flame images, thermocouples, radiometers, and vehicle pressure transducer (not discussed here since it did not vary discernibly during the SIBAL tests). This section will first discuss the flame images and the analysis of those images with respect to flame spread rate (V_f), flame growth, and flame and pyrolysis lengths (L_f and L_p). These measurements are compared to previous flight results. The surface thermocouple data are also compared to previous flight data, and the radiometer data from Saffire IV and V are compared.

3.1 Surface View Flame images

In Fig. 3, the SIBAL sample from Saffire IV is shown where half of the image is green LED-illuminated (right0 and half of it is the enhanced dark flame image (left). The stark contrast between the unburned and pyrolyzed fabric is evident. There are soot streaks across the unburned fabric that were deposited during the ignition sequence. The dark flame image needed significant enhancement to bring out the dim thin flame sheet that is just discernable above the background noise. The flame length appears to be the same length as the pyrolysis front for the SIBAL fabric. The flame base is easily discerned in both images but is best resolved in the illuminated image as a thin pinkish line along the bottom of the sooty region of the flame.

Unburned cotton remaining in the fiberglass matrix continues to smolder as bright spots after the flame base has passed.

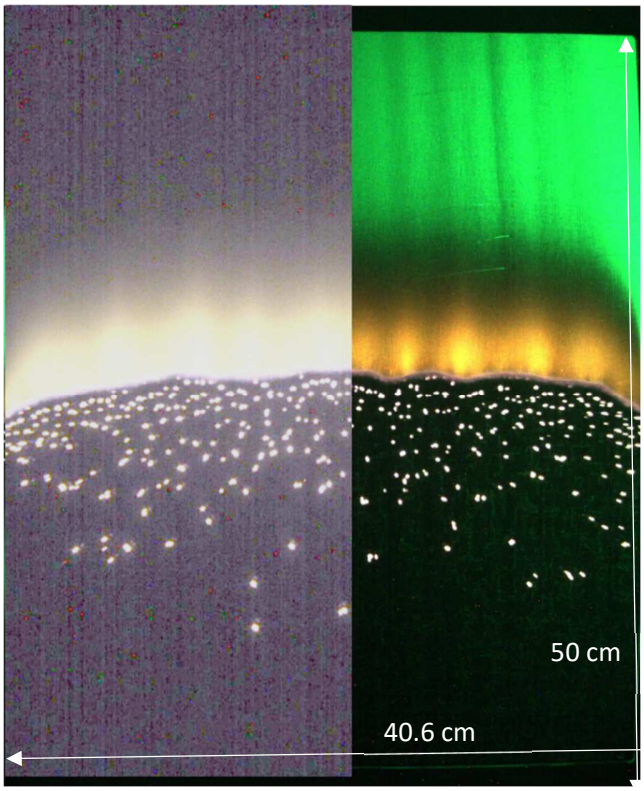

Figure 3: SIBAL fabric from Saffire IV. Left dark background image is brightness enhanced to show the flame and the right image is illuminated with a green LED to reveal the pyrolysis front. The forced flow is upward in these images. Once the flame base has passed, smolder spots are left behind that consume unburned cotton left within the fiberglass matrix.

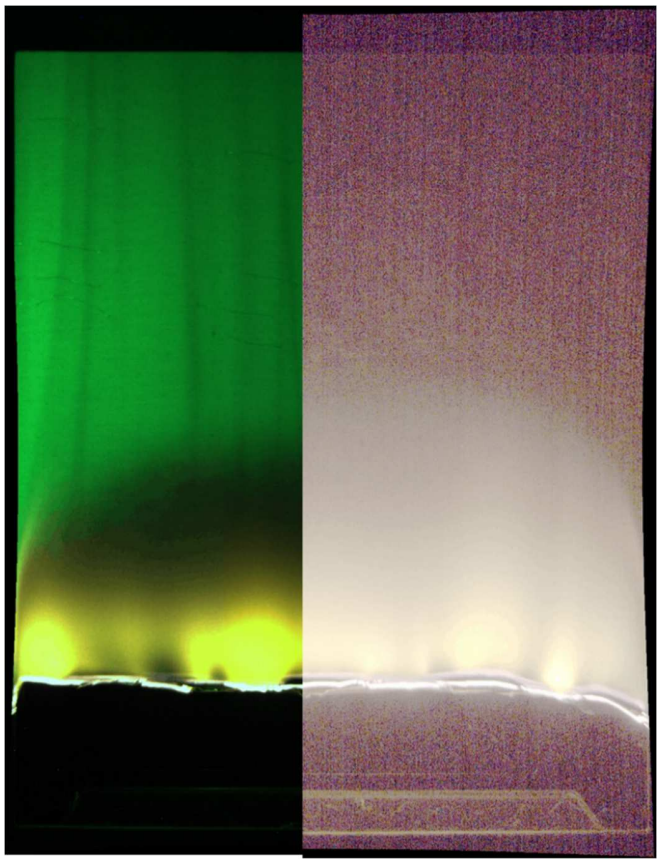

Figure 4: Cotton fabric from Saffire V, with same dimensions as Fig. 3. Left image is externally illuminated, showing pyrolysis front, and right image is the dark background image enhanced to bring out the flame. Note that the fuel burns away unlike the SIBAL fabric. Images were taken earlier in the test than Fig. 2 because the fuel distortion distorted the flame shape later in the test.

The surface view flame images for the cotton sample in Saffire V are shown in Fig. 4. Unlike the SIBAL fabric, the cotton burns away completely, especially over the first half of the sample. The images shown are taken earlier in the test than those shown in Fig. 3 because the cotton sample began to curl up when the flame reached the thermocouple location. The curling sample distorted the flow field and flame shape. One can see the char oxidation is upstream of the flame base in the images, and the oxidation is incomplete, so the residual char builds up the further the flame spreads. The flame length in the dark image is seen to be significantly longer than the illuminated pyrolysis length for the cotton. This may be due to the larger amount of fuel released during pyrolysis for the cotton. Recall the area densities of the two samples are very close, but the SIBAL fabric is 25% inert fiberglass. It may also be due to the different ambient atmosphere.

Figure 5 shows the 5 cm wide sample flame (externally illuminated and dark background). The entire flame shows strong curvature, indicating the flame is three-dimensional in nature with significant edge effects. Also shown are the much narrow BASS images that also show strong curvature. There was no LED in the BASS tests to externally illuminate the pyrolysis front.

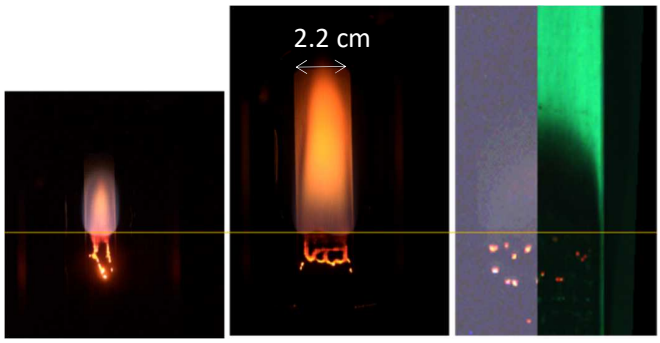

Figure 5: Smaller SIBAL samples: a) 1.1 cm wide; b) 2.2 cm wide; c) 5 cm wide (left dark background, right LED illuminated).

3.2 Edge View Flame Images

Edge view images were obtained for the BASS tests and two of the Saffire flights. The much smaller BASS edge view images are shown in Fig. 6. The 2.2 cm wide sample was long and sooty while the 1.2 cm wide sample was all blue due to the larger fraction of heat loss to the metal sample holder.

The Saffire edge view images have an extreme depth of the flame (~ 40 cm). The lens distortion

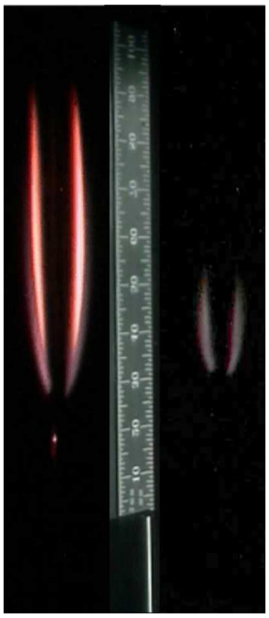

Figure 6: Edge view images of BASS tests with SIBAL fabric. Left 2.2 cm wide sample. Right: 1.2 cm wide sample. Ruler for scale added between images. Conditions are listed in Table 1.

and viewing angle makes quantitative analysis very difficult, but it is still useful to compare the two edge view images in Fig. 7. The flame is easily seen in both views due to the intensity integration across the flame depth. The LED illumination reveals the fuel surface for the SIBAL fabric in these very slightly oblique views. It is challenging to accurately determine the location

of the pyrolysis zone at this angle given that the edges of the material are unburned further upstream than the centerline. The cotton fabric image also has LED illumination, but it is hard to see without enhancing the image. This indicates that the cotton flame is much brighter at the higher oxygen concentration despite the lower pressure at the normoxic atmosphere. This is consistent with the linear dependence with oxygen but a square root dependence on pressure [8]. One cannot see the blue in the flame as the soot intensity dominates the image without enhancement. With enhancement, both blue flame tips are seen to be longer, but the cotton flame is much longer. The SIBAL flame has a tapered flame base since the two sides of the flame are separated by the fiberglass mesh. The cotton flame base is rounded as the flame is wrapped around the exposed base of the fuel. The cotton flame is also thicker than the SIBAL flame due to the reduced pressure.

3.3 Flame tracking

Surface view images were tracked with time using NASA-developed Spotlight software. The dark background and LED-illuminated images were separated and tracked separately using an automated tracking with multiple filtering steps to eliminate noise and enhance the difference between the background and the flame before applying a threshold value to find the edge of the flame. Flame bases was tracked in both dark and illuminated images, and the flame tip at the center of the sample was tracked in the dark background frames that were contrast enhanced to bring out the dim flame tip. The pyrolysis front at the center of the sample was tracked in the

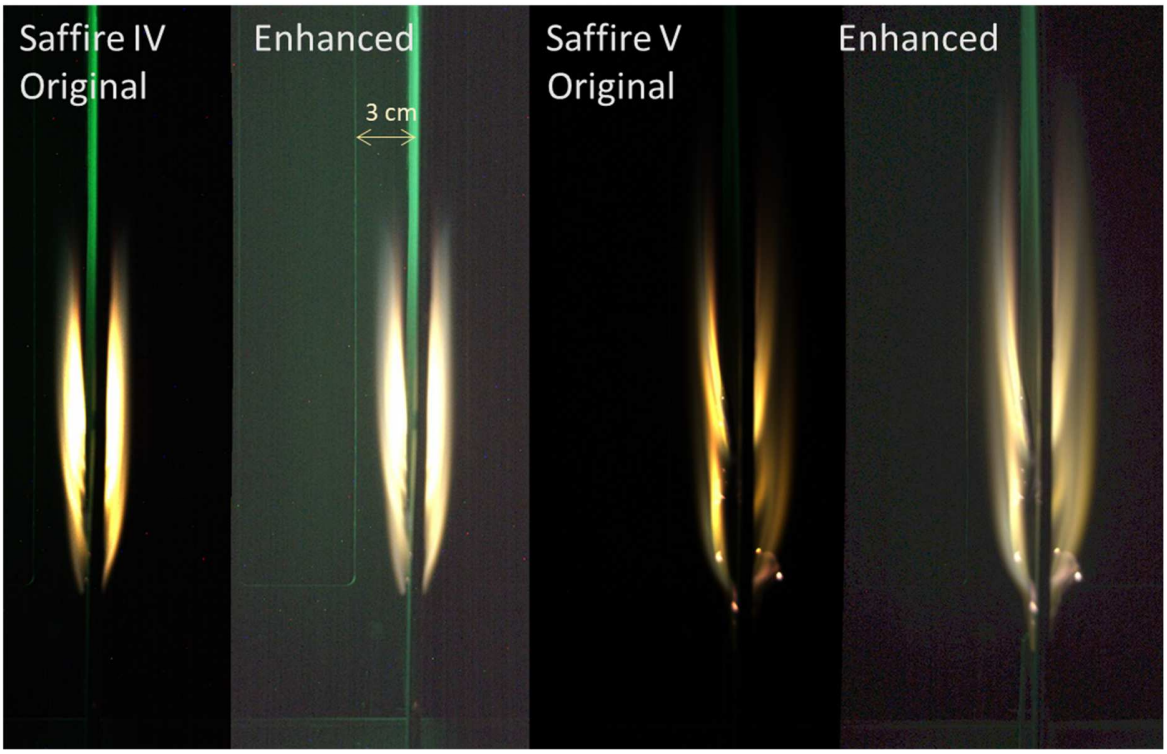

Figure 7: Edge view images from approximately the same flame base position for left two Saffire IV (@58 s) and right two images from Saffire V (@63 s). The left image of each pair is unenhanced, while the right image is the same image with a 2.5 gamma correction applied to bring out the blue flame tips and green LED illumination. The images are cropped to capture the same area of the duct.

illuminated frames. Real-time monitoring of the tracking visually confirmed the accuracy of the tracking. Results are shown in Fig. 8 for both samples.

The SIBAL tracking shows a very steady flame spread that reaches a maximum flame and pyrolysis length of approximately 105 mm early in the flame spread at 30 - 40 s when the flame base is at only 100 mm from the igniter, and the length decreases gradually from there. The flame tip spreads rapidly during the early flame growth phase before slowing down. The flame base propagates steadily throughout the test, and the flame length briefly reach steady state after about 100 s before the tip reaches the end of the sample. This sample was just half the length of the samples burned in Saffire I and Saffire III.

The cotton fabric flame tracking is shown in the bottom graph of Fig. 8. The flame base spread steadily during the early part of the test, and the flame tip spread quickly during the flame growth phase before slowing. Large maximum flame and pyrolysis lengths are also noted early in the test at 40 s, when the flame base is 100 mm from the igniter. The flame size decreased as the test progressed, but after the flame base passed the surface thermocouple at 300 mm, the cotton fabric charring, and curling caused the flame to become non-uniform and the tracking reflects the disturbance in the flame spread. The spread rate was determined from the slope of the base tracking prior to 300 mm (<100 s) (see dotted line on the dark flame base tracking in Fig. 8).

The flame spread rates were similar for the SIBAL fabric in Saffire IV (0.36 cm/s) and cotton in Saffire V (0.34 cm/s) despite the atmosphere differences listed in Table 1. Using the concurrent flame spread correlation $V_f \sim O2\%^* P^{1/2}$ [8, 18, 24] the ratio of spread rates agrees well with the oxygen-square root of pressure ratio for the two tests.

To evaluate the unique difference in flame and pyrolysis length for the cotton sample, the data were fit with a polynomial as shown in Fig. 9. This was necessary as there were many fewer

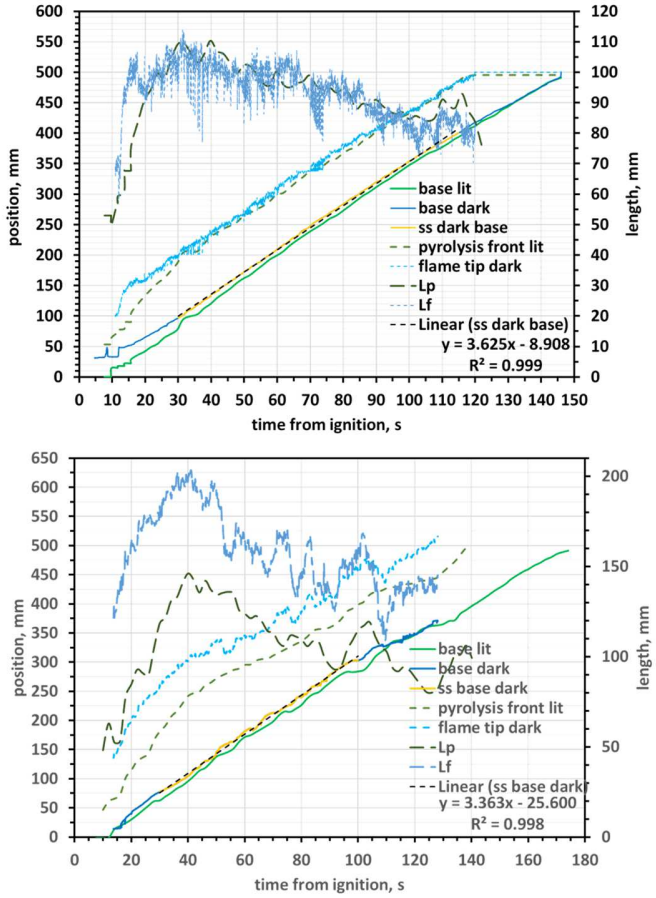

Figure 8: Flame tracking for Saffire IV SIBAL (top) and Saffire V cotton (bottom). The steady flame base position versus time is used to measure the flame spread rate. Both dark background images and LED-illuminated images are tracked. Flame and pyrolysis lengths, L_f and L_p, are graphed from the differences between the base and flame and pyrolysis tip locations.

illuminated frames to measure the pyrolysis length than there were dark frames to measure the flame length. The polynomials were then subtracted to determine the difference in lengths. The difference of 40 mm becomes a constant by roughly 60 s, well before either length becomes steady based on the polynomial fits and the cotton fabric starts to curl (after 100 s).

The cotton flame length is longer than its pyrolysis length while two lengths match for the SIBAL fabric for all SIBAL tests. This may be related to the actual amount of fuel available, which is 25% higher in the cotton material. For similar spread rates, the cotton burning rate is thus higher, resulting in a longer flame due to excess pyrolyzate relative to the SIBAL fuel. The specific heat of the pure cotton is also higher than the SIBAL fabric blend, which would reduce the flame spread rate and increase the preheat length. The lower ambient pressure also increases the flame thickness, which may reduce the heat flux from the flame to the fuel surface in the

preheat region. The hot fiberglass and residual smoldering upstream of the SIBAL fuel flame will provide an extended thermal boundary layer that may also affect the hydrodynamic boundary layer upstream of the flame whereas the flame base for the cotton fuel is exposed to the ambient temperature inviscid core flow.

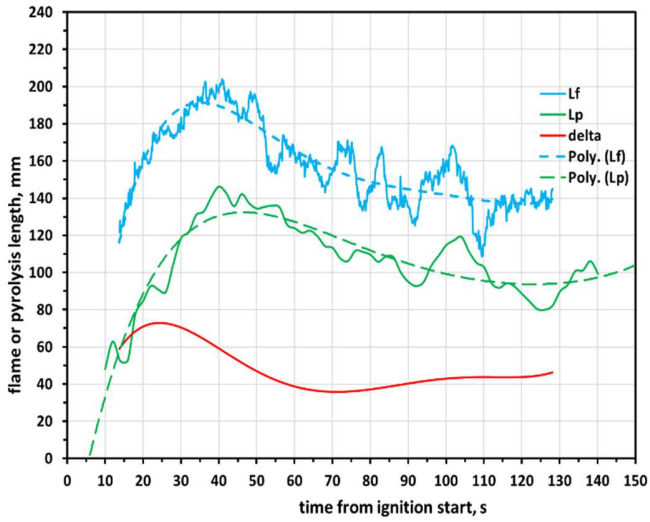

Figure 9: Flame and pyrolysis lengths from cotton sample in Saffire V are fitted with polynomials to calculate the difference in lengths.

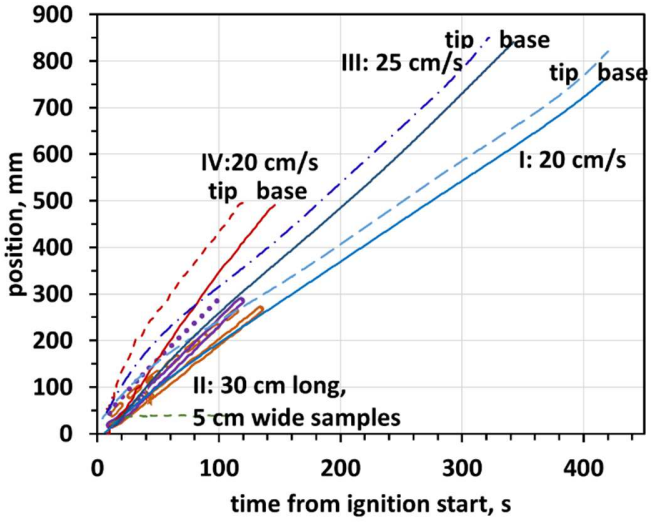

Figure 10: Flame tracking results from Saffire I, II, III in comparison to Saffire IV.

The flame tracking results for Saffire I-III are provided in Fig. 10 for comparison and show similar trends for the wide samples as Saffire IV and V. The spread rates, flame and pyrolysis lengths, and sample and duct sizes for all 5 flights are reported in Table 1.

3.4 Pyrolysis length comparisons

The pyrolysis lengths for all 5 flights are shown in Fig. 11. As indicated by the red first vertical dashed line, the pyrolysis lengths for all but the 5 cm wide samples reach a peak at ~ 40 s. The 5 cm wide samples appear to reach a steady size at approximately that time. The purple second vertical dashed line indicates that the longest full width samples reach a steady state pyrolysis length by approximately 100 s. Saffire IV appears to be plateauing at approximately the same time but both Saffire IV and V were too short to clearly show the plateau. The cotton sample also began to curl later in the test, further distorting the measurement of the pyrolysis length.

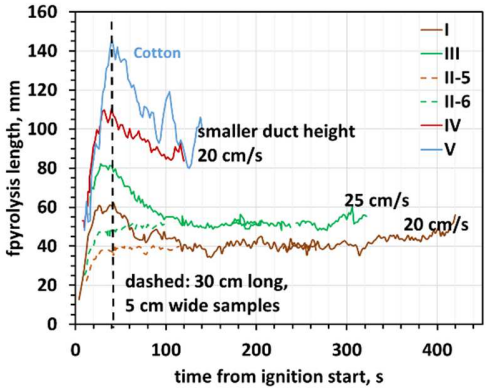

Figure 11: pyrolysis length histories from Saffire I-V.

Saffire I and III had strong transient excess pyrolysis lengths (overshoots) while the smaller Saffire II samples did not. The BASS samples also did not [12]. The small samples do not exhibit a similar excess length because 1) the flame is deep within the boundary layer half-way down the duct for Saffire II, 2) there is room for the thermal expansion to expand laterally as well as downstream for both Saffire II and BASS samples, and 3) oxygen can diffuse from the sides as well as from above these three-dimensional flames, all of which allows the flames to smoothly grow to their steady size. The comparable velocity tests in Saffire II did indeed smoothly plateau to the same steady-state pyrolysis lengths as Saffire I and III by 100 s.

Using the spread rates V_f for each test, the pyrolysis length L_p history can be converted into the burnout time t_b history using $t_b=L_p/V_f$. As shown in Fig. 12, the SIBAL burnout time histories from flights I, III, IV collapse nicely. The burnout time linearly increases with time after ignition (nearly 1:1) until the peak value, after which there is a slow decay in burnout time until a steady value is obtained for the longer tests. This can be called the transient excess burnout time, in parallel with the transient excess pyrolysis length. The burnout time histories from the smaller Saffire II samples 5 and 6 asymptote to the steady values due to more effective oxygen transport across the narrow samples resulting in a larger heat feedback to the sample [17]. The steady state burnout time for SIBAL in atmospheric air appears to be approximately 22 s.

The cotton fabric exhibited a similar but larger transient excess pyrolysis length as the SIBAL fabric, which clearly shows that the transient excess pyrolysis length is not solely due to the flame base spreading into an increasing boundary layer [17]. The cotton sample burns away (removing the no-slip condition at the center plane) and the flame base is exposed to the inviscid core flow within the duct, so some factor other than just the boundary layer development needs to account for this observation.

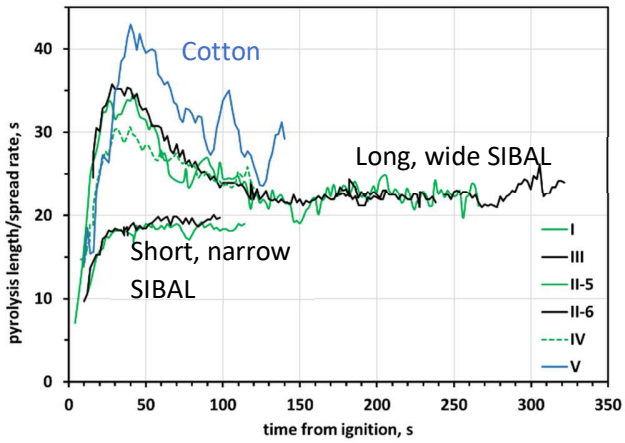

Figure 12: Burnout time history for each Saffire test

Saffire V (cotton), which does not have a boundary layer upstream of the flame due to complete fuel burnout, had the largest transient excess in burnout time, as shown in Fig. 12, possibly due to the higher burning rate of the fuel as mentioned previously. The time from ignition to the transient excess maximum (~ 35 s) was consistent for the SIBAL samples, while the cotton maximum occurred slightly later (~ 40 s) also due to the higher burning rate of the fuel. The oxygen and pressure differences for the cotton test may also play a role in the magnitude and timing of the maximum excess burnout time.

Saffire IV, with a smaller duct than Saffire I, had a slightly smaller transient excess maximum burnout time (burnout time peak ~ 30 s versus ~35 s for Saffire I and III) because the inviscid core flow was faster (as will be shown in Section 4.0, resulting in a faster spread rate which promotes faster developing preheat and pyrolysis regions. The actual maximum excess pyrolysis length is larger, also due to the faster inviscid core flow. To better understand the transient excess pyrolysis lengths, we next look at the surface thermocouple data.

3.5 Thermocouples

Type K thermocouples were used to measure the fuel surface temperature. Thermocouple locations are given in Table 1 for each of the Saffire flights. The SIBAL thermocouple data were aligned so that burnout occurs at x=0 in Fig. 13a. The pyrolysis temperature is 400°C where the temperature traces change slope. Except for the small samples from Saffire II, the traces are similar, with Saffire I and III being very close while Saffire IV has a slightly longer preheat time.

Using the flame spread rate, the time is converted to distance from burnout in Fig. 13b. Plotted this way, Saffire IV really stands out from the other tests where it shows a much longer preheat length consistent with a higher inviscid core flow velocity in the smaller duct. The sample length and thermocouple locations were not adequate to fully capture the early preheating but did capture the longer pyrolysis length of 85 mm as listed in Table 1. Saffire I and III, on the other hand, do capture the early preheating for the downstream-most thermocouple for the larger samples and Saffire I-III all have similar pyrolysis lengths (40 mm for 20 cm/s and 50 mm for 25 cm/s tests).

The x-axis distance is normalized by the pyrolysis length in Fig. 13c. The x-axis can also be interpreted as t/t_b since time was multiplied by V_f and then divided by L_p to derive the axis. The onset of pyrolysis is at unity non-dimensional burnout time. This implies that the burnout time is associated primarily with the pyrolysis time, and not the preheat time which varies for the different tests in Fig. 13c. The transient excess pyrolysis length may thus be associated with changes in the heat flux primarily in the pyrolysis zone more so than in the preheat length.

In Fig. 13c, it becomes more obvious that Saffire IV also had a higher pyrolysis temperature across the pyrolysis region. This may be due to the higher inviscid core flow velocity with the shorter duct height, which would increase the heat flux to the fuel. It may also be partially due to the lower humidity level of the air during Saffire IV compared to the other flights (37% RH on Saffire IV, while 47%, 45%, and 46% RH for Saffire I, II, and III, respectively). The hydrophilic cellulose in the fuel samples hydrogen bonds with the water, and the higher the humidity, the more of the flame heat flux must go into vaporizing the bonded water.

The cotton surface temperature profile is compared to the SIBAL temperatures in Fig. 14. In Fig. 14a, the cotton and SIBAL surface temperatures are compared from Saffire IV and V as a function of distance from burnout. While the preheat lengths appear similar, the cotton fabric exhibits an extended pyrolysis length compared to the SIBAL for the thermocouples the same

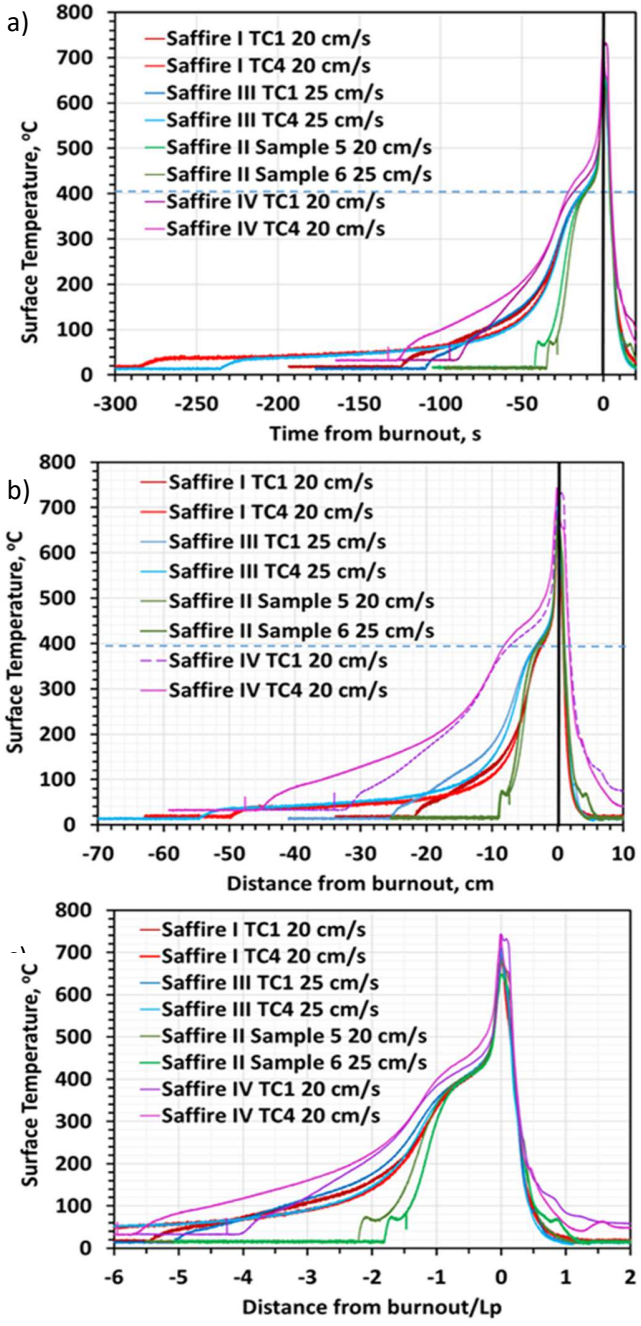

Figure 13: Thermocouple data a) with time from burnout; b) with distance from burnout; and c) non-dimensional distance from burnout, which can also be thought of as t/t_b.

distance from the igniter, which is likely due to the large transient excess pyrolysis length observed. In Fig. 14b, the surface temperatures are compared as a function of non-dimensional pyrolysis length or equivalently, the non-dimensional burnout time. A transient pyrolysis length was used in this analysis since the flame passes over the thermocouple during the transient phase of the flame development. A pyrolysis length of 160 mm was taken at 60 s in Fig. 9 where the pyrolysis tip from the illuminated images passes over the thermocouple at 30 cm downstream of the igniter. The difference between flame length and pyrolysis length had just stabilized to the steady difference at 60 s as shown in Fig. 9. The further downstream thermocouple was not usable due to char curling distorting the flame and flow.

While the SIBAL surface temperature increased steadily after the pyrolysis started, the cotton fabric plateaued for an extended length at the 400°C pyrolysis temperature until the burnout spike in temperature. This is attributed to the fiberglass inert material in SIBAL that can continue to heat while the cotton pyrolyzes at a fixed temperature. Post-burnout, the curling cotton fabric char remains tangled with the thermocouple leads as reflected in the jagged temperature data for

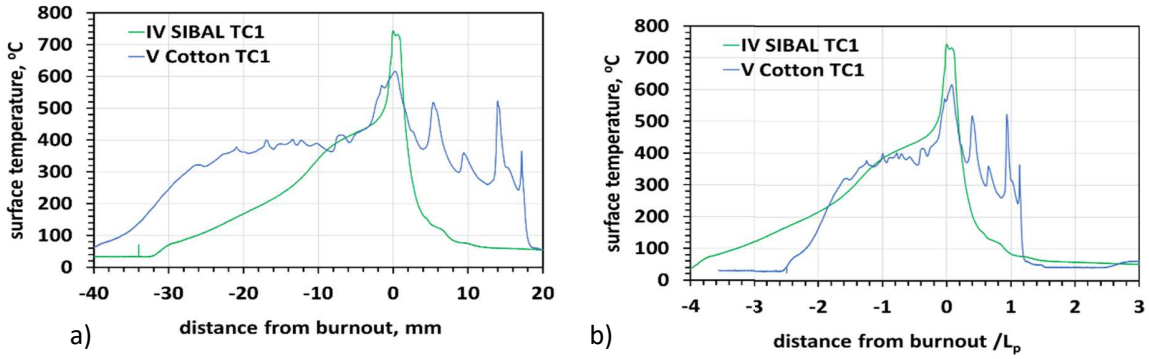

Figure 14: surface temperature profiles for SIBAL and cotton from Saffire IV and V, respectively. a) time converted to distance from burnout, b) time converted to x/L_p or t/t_b.

positive distances relative to burnout.

4. Discussion

4.1 Heat flux and burning rate estimates

The surface thermocouple data can be used to estimate the heat flux using the Eq. (1) surface

$$\dot{q}_f'' = \rho_s \tau_s(t) C_s(t) \frac{dT_s}{dt} + \varepsilon\sigma(T_s^4 - T_\infty^4) + L_v(T) m_s(t) A_s e^{-E_s/RT_s}$$

energy balance:

Here, the heat flux from each side of the flame $\dot{q}_f''$ is equal to the heat up of the fuel, the re-radiation from the fuel surface, latent heat of vaporization of the fuel using a first order pyrolysis model, and conduction in the solid from the pyrolysis zone to the unheated fuel. The downstream

□ondu□tion term □an be negle□ted for □on□urrent flame spread be□ause the □ondu□tive heat transfer along the burning thin solid material is mu□h smaller than the □onve□tive heat transfer asso□iated with the gas flow velo□ity parallel to the □ombustible surfa□e for the velo□ities studied in this work. The initial half-thi□kness area density $\rho_s \tau_s$(t) is 0.009 g/□m^2 initially but de□reases as the □otton is vaporized, the spe□ifi□heat C_s(t)is □al□ulated by weight-averaging the fiberglass (0.7 J/g K) and □otton heat □apa□ities (1.26 J/g K) where the □otton fra□tion de□reases as the □otton is vaporized), the emissivity ε is taken to be 0.8, the experimental Stefan-Boltzmann □onstant σ is 5.729 x 10^{-8} W/m^{2}K^4, the latent heat L_v = 300 +($C_{p,f}$ – C_s)(T_s-300) J/g [31] and kineti□parameters A_s= 1.626 x 10^{11} s^{-1}, E_s = 1.6144 x 10^5 J/mol, and R = 8.3145 J/mol K [30].

Since all the SIBAL fabric thermocouples scale similarly as shown in Fig. 13c, the test with the longest preheat history recorded by a surface thermocouple is used to estimate the heat flux from the flame in the preheat region. This test is Saffire I due to its slow flame spread rate. The temperature-time data is shown in Fig. 15a for the furthest downstream surface thermocouple. The surface temperature data is curve-fit using a polynomial which provides a coefficient of determination very close to unity. This polynomial is differentiated to get a smooth dT_s/dt for the first term in Eq. (1).

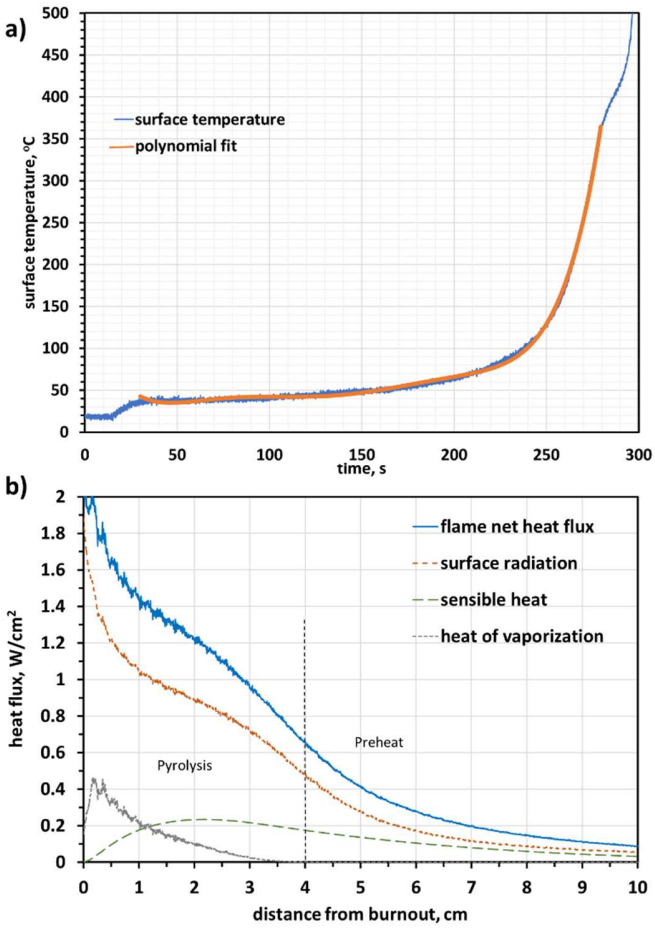

Figure 15: a) Saffire I surface temperature history; b) heat flux from Eq. (1) ahead of the pyrolysis front.

The resulting flame net heat flux estimate and each contributing term from Eq. (1) is shown in Fig. 15b, where time has been converted to distance from the burnout (flame base) using the spread rate. The heat flux rises slowly far ahead of the flame but increases rapidly within a few centimeters of the flame base. Defining the preheat length to be the distance from the onset of pyrolysis to the point where the net heat flux dropped to ~10% of the heat flux at the onset of pyrolysis [9], the preheat length is ~10 cm. At steady state at 100 s, the Saffire I flame base was at 20 cm. The pyrolysis length for this test was only about 4 cm, so the preheat length is 2.5 times as long as the pyrolysis length.

The heat flux at the pyrolysis front is in the range of the critical heat flux for ignition of cellulose (1-1.3 W/cm^2, [32]). The general shape of the net heat flux agrees with the model [17] although the model predicts a peak near 1 W/cm^2 (0.25 cal/s cm^2) at the flame base instead of near the pyrolysis front. Radiation and sensible heat take up the flame heat flux in the preheat region. The latent heat of vaporization only becomes larger than the sensible heat in the last centimeter before burnout. At burnout, all the flame heat flux goes out as re-radiation.

4.2 Duct size effects

As shown in Table 1, three different duct sizes and five different sample sizes have been tested. The spread rate data [3] is different for each duct and SIBAL fuel sample size for the same forced flow velocity. As shown in Fig. 16, the flame spread rate increases as duct height decreases except for the narrow BASS sample, where lateral heat losses to the holder may have slowed the flame. The flame in the Saffire IV 30.5 cm tall duct had a steady spread rate and pyrolysis length that were twice that of the flame in the 51 cm tall duct for Saffire I. The spread rates and pyrolysis lengths are predicted [19] to decay as the inverse of the duct height for ducts between 4 cm and 9 cm tall, so it is surprising that such large ducts show such a dramatic difference. It seems clear from the preceding sections that the flame is sensitive to the duct geometry (height, aspect ratio, length), sample geometry and burning behavior (sample width, complete burnout, or residual fiberglass matrix upstream) and the size of the flame within the duct, which may be a function of the ambient oxygen concentration, pressure, average flow

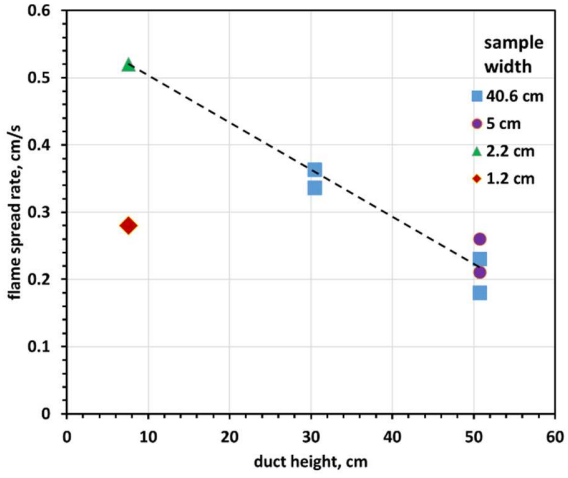

Figure 16: Effect of duct and sample size on the flame spread rate. BASS samples were in the smallest duct while Saffire samples were in the larger two ducts.

velocity, and fuel area density.

Boundary layer, thermal expansion, and lateral oxygen diffusion effects have been shown in numerical model predictions [17]. For example, in their Fig. 6, Li et al. [17] show streamlines, oxygen concentrations, and reaction rate contours for wide versus narrow samples at 3 heights above the fuel surface. Notably, the oxygen deficit at all heights for the wide sample is much more significant than the narrow sample. The flow diversion around the flame is similarly stronger for wide samples at 0.9 cm above the fuel surface while narrow sample the flow streamlines are straightening. The reaction contours show the 0.0001 contour has a similar wing-like shape at 0.3 cm for both widths, but at 0.6 cm the narrow sample has a much thicker (in the flow direction) 0.0001 contour for the narrow sample. It isn't until 0.9 cm that the wide sample develops a thicker reaction zone at that level.

The model [17] also predicted a gradually decreasing pyrolysis length as the flame spreads into the thickening boundary layer, which is not observed in any of the long sample tests (Saffire I and III) where this effect would most likely have been observed. This may be due to exit boundary condition differences between the model and the experiment.

The transient excess pyrolysis length observed in the Saffire experiments is hypothesized to be caused by a post-ignition flame growth transient where, due to the initial lack of pyrolysis and preheated regions, the time it takes for the fuel to burn out gets very long until these regions can develop. This is consistent with two-dimensional transient model predictions [16] where the transient excess pyrolysis length (i.e., 'overshoot') is described as follows: "In thin solids, almost all the heat input comes from the gas phase and is equal to the product of the average heat flux per unit area and the preheat length. Initially, the heat flux is high and the preheat length is small. Later, the preheat length becomes large but the heat flux diminishes. The product of the two results in a peak during the flame growth process". This description is consistent with the burnout time histories shown in Fig. 12.

4.3 Flow Acceleration Estimates

The following analysis is intended to analytically correlate the flame spread rate with effective flow velocity (U_e) by taking the duct size and flame size into account to estimate the effective flow velocity for each configuration. Two different effects will be considered: flame thermal expansion causing flow acceleration and developing boundary layers causing additional inviscid core flow acceleration. The inlet flow to the duct is assumed to be fixed and not affected by the flame or boundary layer growth on the surface. Saffire V is included but we point out that the cotton fabric fuel burns away and there is no boundary layer over the sample holder except the first 3 cm of the sample card, which is neglected in the analysis. In addition, pressure, oxygen, and fuel type are different in Saffire V, which may also confound the spread rate correlation even though the partial pressure of oxygen is close to the atmospheric air ambient of the other tests.

Thermal expansion creates two effects as predicted in Fig. 5a from the numerical model [17]. The first is the creation of a high local pressure plateau that retards the incoming flow and changing the local flow at the flame base by diverting the incoming streamlines at the flame base (a drag effect similar to a porous body). This may affect the flame spread rate. The second is to

accelerate the flow inside the flame. The flow acceleration may strongly affect the preheat zone, which is located downstream of the flame, especially in a smaller chamber. Both will be affected by the sample size relative to that of the chamber.

The flame thermal expansion is simply estimated assuming isobaric thermal expansion of an ideal gas using the flame volume and average temperature to estimate the gas expansion of that volume. The flame is treated like a box of dimensions L_f x w x $2H_f$ for simplicity, where the visible flame height H_f is doubled to estimate both the inner half and outer half of the flames' thermal field. The average flame temperature is assumed to be T_{mean} = 1050 K for a flame temperature of 1400 K based on 8 mm and 1 cm thermocouple readings from Saffire I, III, and IV, and a pyrolysis temperature of 700 K.

The increase in thermal expansion volume V_e for both sides of the sample is estimated using Charles's Law in Eq. (2) as

$$V_e = L_f * w * 2 * 2 * H_f * \frac{T_{mean}}{T_\infty} \qquad Eq.(2)$$

The only non-measured value is the height of the flame H_f (meaning the outer standoff of the visible flame) for Saffire I-II because no side view cameras were used on those flights. Educated guess values are used for those flights as indicated in Table 1.

The velocity increase through the duct due to the thermal expansion U_e is estimated in Eq. (3) based on the fractional increased gas volume for a constant pressure as

$$U_e A_{duct} = \frac{(V_e + V_{duct})}{V_{duct}} * UA_{duct} \qquad Eq.(3)$$

Since the duct area is fixed and appears on both sides of Eq. (3), it cancels out. The smallest flames in the largest ducts showed negligible core flow acceleration due to thermal expansion. However, the thermal expansion increased the core flow by 113% for the largest flames, and that effect will occur locally and move with the flame. This may counteract to some extent the growing boundary layer over the sample as "the flame disturbs the flow" [17]. This may help explain why steady flame lengths are observed instead of a slowly decaying length [17].

The second factor is the impact of developing boundary layers on the flow. As the flame moves down the SIBAL sample, the flame moves into an increasing boundary layer. The centers of the samples are located at between 0.7 and 1.1 L/D_H, where D_H is the hydraulic diameter of the ducts. This is clearly in the entrance length region of the ducts (10-13% of the entrance length using the correlation $E_L/D_H = 0.06\ Re_D$). The flow away from the surfaces is thus an inviscid core flow, and boundary layer growth from the 4 duct walls and 2 sample surfaces causes a core flow acceleration down the duct as well.

We estimate the flat plate boundary layer thickness δ as a function of the distance x along the sample using Eq. (4).

$$\delta = 5\left(\frac{\nu x}{U_e}\right)^{1/2} \quad Eq.\ (4)$$

One third of the volume of all the boundary layers (V_{BL}) is assumed to go into accelerating the core flow (displacement thickness $\delta^* \sim \delta(x)/3$ for a flat plate boundary layer). Since the core flow is inviscid, we can simply add the volumes (superposition of potential flows).This volume for both sides of the sample, the top and bottom walls, and the side walls (neglecting corner effects) is approximated in Eq. (5) as

$$V_{BL} = \sum_{x=0}^{x=L_{holder}} \frac{\delta(x)}{3} * (w\Delta x * 2) + \sum_{x=0}^{x=L_{duct}} \frac{\delta(x)}{3} * (W\Delta x * 2) + \sum_{x=0}^{x=L_{duct}} \frac{\delta(x)}{3} * (H\Delta x * 2) \quad Eq.(5)$$

In each discrete summation, the sample and duct dimensions are taken from Table 1. The Δx used is 0.1 cm.

Note that we do not have a boundary layer on the cotton fabric since it burns away, so the first term in Eq. (5) is zero for the cotton fabric test, neglecting the small 3.3 cm long upstream sample card. Equation (5) calculates the total displacement throughout the whole duct, but the displacement increases as the flow moves through the duct, so the core flow will accelerate as it

moves through the duct.

The impact of the boundary layers needs to be iterated since the increased core velocity due to the boundary layer flow displacement (U_{BL}) is estimated in Eq. (6), where the displaced volume is subtracted from the duct volume in the denominator. This accounts for both thermal expansion and the boundary layer displacement, and then the boundary layer displacement is updated using Eq. (5) and Eq. (7). The process is repeated n times until the result converges to a constant value when n=4 in Eq. (6).

$$U_{BL_n} = \frac{V_{duct}}{V_{duct} - V_{BL_n}} * Ue \qquad Eq.(6)$$

$$\delta_n = 5\left(\frac{\nu x}{U_{BL_n}}\right)^{1/2} \quad Eq.\ (7)$$

The core flow velocity increase due to the volume displaced by the boundary layers varies from 112% of the initial duct volume for the largest duct to 135% for the BASS duct. The increasing inviscid core flow velocity as the flow moves through the duct will result in increased momentum and heat transfer [33] which might offset to some extent the predicted decay in pyrolysis length with time [17] as the flame moves into an increasing boundary layer.

The resulting correlation between flame spread rate and the accelerated flow U_{BL4} is shown in Fig. 17. The linear fit is for all the 20 cm/s tests, including the cotton test, with a reasonable coefficient of determination despite the basic approximations made in this scaling analysis.

However, the 25 cm/s tests do not correlate well. There may be additional interactions between the thermal expansion and boundary layer core flow acceleration that are ignored in this simple estimate. For example, the thermal expansion occurs locally around the flame where the flow is

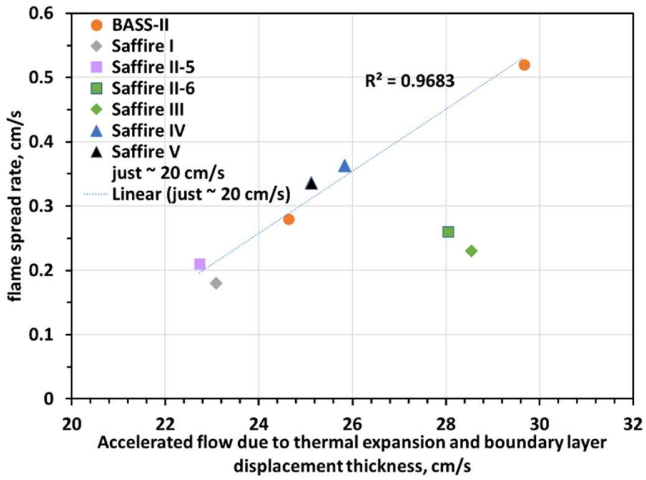

Figure 17: Flame spread rate as a function of accelerated flow for all tests. The linear correlation does not include the 25 cm/s tests.

diverted around the flame [17, 18]. The flame disrupts the boundary layer, so it may be that the differences in the local flow between 20 cm/s and 25 cm/s are small. Figure 5 from [18] shows the local velocity upstream of the flame base is very small relative to the freestream velocity. Indeed, if the Saffire II-6 and Saffire III 25 cm/s accelerated flows were set to be equal to the 20 cm/s accelerated flows for Saffire I and Saffire II-5 (to make them the same locally) in Fig. 17, the data would line up very well with the other data. The 5 cm wide Saffire II tests have faster spread rates than their comparable full width sample tests, possibly due to the lateral oxygen transport possible with the small samples [17].

The effect of duct size is most easily seen by comparing Saffire IV and Saffire I. With the smaller duct, the core flow acceleration is higher, resulting in a higher flame spread rate. The 2.2 cm wide BASS test in the very small duct had the most core flow acceleration and the highest spread rate despite being a much smaller flame, so the duct size affects the flame more than flame size.

As discussed in Section 3.3, the cotton test had the largest maximum transient excess pyrolysis length (overshoot) and longest burnout time maximum. This indicates that a flame moving into a boundary layer along the fuel surface is not required to observe this transient since the cotton burns away and there is no boundary layer upstream of the flame base. Some other process must cause this early transient. It is suggested here that for the full width samples, the inviscid core flow acceleration due to thermal expansion and boundary layer growth (on the walls) creates a very long flame until the preheat and pyrolysis lengths develop, and the burnout time can reach a steady value. For the narrow samples (BASS and Saffire II), lateral expansion and lateral oxygen transport can reduce the flow acceleration effect and allow a smooth three-dimensional flame growth.

The boundary layer on the sample grows along the sample length and its changing thickness can affect the local velocity felt at the flame base. Using the flat plate Blasius boundary layer solution, we can graph the forced flow velocity at the flame base (y=0.2 cm above the fuel surface) for a kinematic viscosity of 0.16 cm^2/s. We use the increased velocity due to thermal expansion U_{BL4} to estimate the boundary layers.

Using Eq. (7) for n=4 and y=0.2 cm as a flame standoff distance, we solve for x using the Blasius boundary layer thickness via Eq. (8).

$$\eta = y\left(\frac{U_{BL_n}}{\nu x}\right)^{1/2} \quad Eq.(8)$$

Figure 18 plots the local velocity at the flame base (stabilization zone) and the boundary layer thickness along the sample length. The local flow velocity in the stabilization zone drops precipitously in the first 10 cm of the sample length as the boundary layer grows. The velocity at the flame base away from the leading edge of the sample holder is quite low for the SIBAL

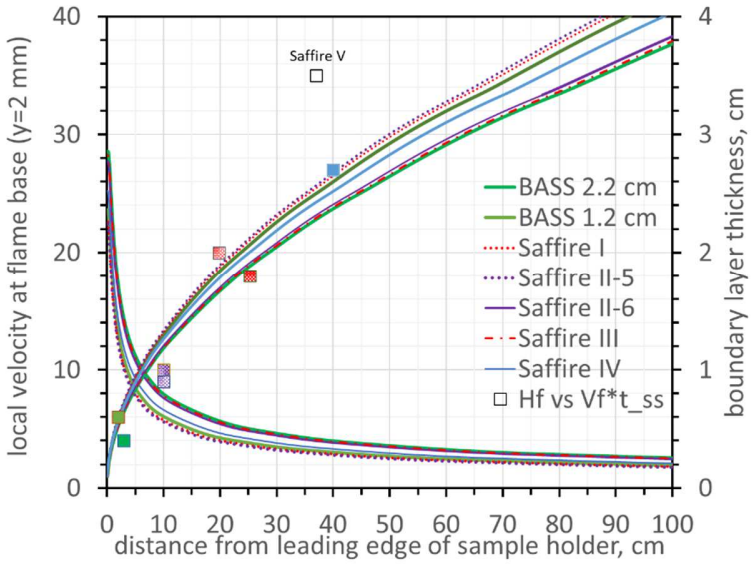

Figure 18: On the left axis is the local flow velocity at the flame base and on the right axis is the boundary layer thickness along the sample length calculated using Eq. (4) and Eq. (5). The flame heights from Table 1 are also plotted at the distance along the sample holder where the flames reached a steady state size, based on data from Fig. 11.

fabrics.

Also included in Fig. 18 is the flame height data from Table 1 plotted at the downstream distance of the flame base (V_f x t_{ss}) which uses the time when the pyrolysis length stabilized (t_{ss}) from Fig. 11. For the full width samples, this was at about 110 s. For the 5 cm wide samples it occurred much earlier since the flames were in a boundary layer flow from the start of the test. The BASS flames stabilized very quickly for the small samples. The flame height data follows the boundary layer thickness quite well.

5. Conclusions

The Saffire IV and V flight experiments recently flew SIBAL and cotton samples (40 cm wide by 50 cm long) to compare the results with the results from the 40 cm wide by 90 cm long SIBAL samples from flights I-III, which were carried out in a larger duct as well as with the results of the much smaller samples and duct in BASS. In the smaller duct used for Saffire IV and V (30.5 cm tall), the steady flame spread rate over the shorter SIBAL sample was twice as fast as in the larger duct (51 cm tall). The flame and pyrolysis lengths were also approximately twice the length of those obtained for the similar experiment in the larger duct. Such dramatic changes in flame behavior for these large ducts was not expected.

The effect of the normoxic atmosphere change on the spread rate between Saffire IV and V is consistent with previously found dependencies on oxygen content and pressure. The specific heat of cotton is slightly higher than SIBAL, which will reduce the flame spread rate and increase the preheat length. In addition, there is more fuel present in the pure cotton, so the flame length should be longer for similar spread rates (higher burning rate). These material differences may explain the difference in flame and pyrolysis lengths for the cotton fabric.

The maximum transient excess pyrolysis length (i.e., overshoot) was also approximately twice as large in the smaller duct for the SIBAL fabric. The cotton fabric, which burns away, also had a large maximum transient excess pyrolysis length, so this excess length is not solely caused by the flame moving into the developing boundary layer thickness on the sample.

The burnout time, defined as the pyrolysis length divided by the flame spread rate, plotted with time collapsed the SIBAL burnout time histories into a single curve with a steady burnout time of approximately 22 s. The transient excess pyrolysis length is believed to be caused by a post-ignition flame growth transient where the burnout time becomes very long until the preheat and pyrolysis lengths develop.

Thermocouple data from the tests indicate that if the position relative to the sample burnout is nondimensionalized with respect to the pyrolysis length, the temperature profiles for all the Saffire SIBAL samples exhibit the same shape across the non-dimensional pyrolysis zone, which can also be interpreted as a non-dimensional burnout time. The preheat length is estimated to be 10 cm as defined as heat flux dropping to 10% of that at the start of pyrolysis, which is 2.5 times longer than the 4 cm pyrolysis length.

A simple surface energy balance in the preheat region reveals that the heat flux rises slowly far downstream of the flame but increases rapidly once within a few centimeters of the pyrolysis front and continues to increase until burnout. In the preheat region, the heat flux from the flame goes into heating the material to the point where surface radiative loss balances the incoming heat flux. The heat flux near the pyrolysis front is in the range of the critical heat flux for ignition of cellulose at the onset of pyrolysis.

A simple estimate of the acceleration of the inviscid core flow in the duct due to thermal expansion and developing boundary layers on the duct walls and the SIBAL sample seems to explain the observed spread rate trends across three duct sizes and multiple sample sizes. The

inviscid core flow increased by 112% and 135% for the largest and smallest ducts, respectively. Thermal expansion depends strongly on flame size and varied from a negligible effect to a flow increase of 113%. The role of lateral oxygen transport also appears to be an important factor despite the relatively high forced flow velocities. These results show there is clearly more to learn about fire growth in microgravity.

Acknowledgements

The authors acknowledge the support of the NASA Mars Campaign Development Division, Exploration Capabilities Office for the sponsorship of the Spacecraft Fire Safety Demonstration Project and the Saffire experiments. In addition, the authors acknowledge the support of the various international space and research agencies that have supported this work including JAXA, ESA, RSA, CNES, DLR, the Russian Academy of Sciences and NASA. The excellent support by the engineering team (NASA and Zin Technologies), Northrup Grumman and the on-orbit crew are gratefully acknowledged. CWRU acknowledges funding by NASA Glenn Research Center under Award #NNX16AL61A and Award #80NSSC22M0011. The European authors would like to express their gratitude to the support from the topical team on fire safety in space (ESTEC contract number 40-0010-3397).
The Russian work was supported by the subsidy from Ministry of Science and Education of the Russian Federation given to the Federal Science Center Scientific Research Institute for System Analysis of the Russian Academy of Science to implement the assignment on the topic No. 0580-2021-0021 “Development of algorithms and codes for multiscale processes and combustion simulations”.

References

[1] G. Jomaas, J.L. Torero, C. Eigenbrod, J. Niehaus, S.L. Olson, P.V. Ferkul, G. Legros, A.C. Fernandez-Pello, A.J. Cowlard, S. Rouvreau, N. Smirnov, O. Fujita, J.S. T’ien, G.A. Ruff, D.L. Urban, Fire safety in space–beyond flammability testing of small samples, Acta Astronaut. 109 (2015) 208-216.

[2] P. Ferkul, S. Olson, D. Urban, G. Ruff, J. Easton, J. T'ien, Y.T. Liao, A.C. Fernandez-Pello, J. Torero, C. Eigenbrod, G. Legros, Results of large-scale spacecraft flammability tests. 47th International Conference on Environmental Systems (2017), ICES 2017-224.

[3] D.L. Urban, P. Ferkul, S. Olson, G.A. Ruff, J. Easton, J.S. T’ien, Y.T.T Liao, C. Li, C. Fernandez-Pello, J.L. Torero, G. Legros, C. Eigenbrod, N. Smirnov, O. Fujita, S. Rouvreau, B. Toth, G. Jomaas, Flame spread: effects of microgravity and scale, Combust. Flame 199 (2019) 168-182.

[4] D.L. Urban, G.A. Ruff, P. Ferkul, J. Easton, J. Owens, S. Olson, M. Meyer, C. Fortenberry, J. Brooker, J. Graf, M. Casteel, B. Toth, F. Meyer C. Eigenbrod, J.S. T'ien, Y.-T. Liao, A.C. Fernandez-Pello, G. Legros, A. Guibaud, N. Smirnov, O. Fujita, G. Jomaas, Fire Safety Implications of Preliminary Results from Saffire IV and V Experiments on Large Scale Spacecraft Fires, 50th International Conference on Environmental Systems (2021), ICES- 2021-266.

[5] G.H. Markstein, J. de Ris, Upward fire spread over textiles, Symp. (Int.) Combust. 14 (1973) 1085-1097.

[6] L. Chu, C.H. Chen, J.S. T’ien, Upward Spreading Flames over Paper Samples, ASME 81-WA/HT-42 (1981) 1-8.

[7] G.D. Grayson, K.R. Sacksteder, P.V. Ferkul, J.S. T’ien, Flame spreading over a thin solid in low-speed concurrent flow-drop tower experimental results and comparison with theory, Microgravity Sci. Tec. 7 (1994) 187-195.

[8] S.L. Olson, F.J. Miller, Experimental comparison of opposed and concurrent flame spread in a forced convective microgravity environment, Proc. Combust. Inst. 32 (2009) 2445-2452.

[9] P.V. Ferkul, J.S. T'ien, A model of low-speed concurrent flow flame spread over a thin fuel, Combust. Sci. Technol. 99 (1994) 345-370.
[10] C.-B. Jiang, J.S. T'ien, Numerical Computation of Flame Spread over a Thin Solid in Forced Concurrent Flow with Gas-Phase Radiation, Fall Technical Meeting of the Easter States Section of the Combustion Institute, also NASA CR-202813 (1994) 1-2.
[11] C. Di Blasi, Influences of sample thickness on the early transient stages of concurrent flame spread and solid burning, Fire Safety J. 25 (1995) 287-304.
[12] X. Zhao, J.S. T'ien, A three-dimensional transient model for flame growth and extinction in concurrent flows, Combust. Flame 162 (2015) 1829-1839.
[13] H.-Y. Shih, J.S. T'ien, Modeling wall influence on solid-fuel flame spread in a flow tunnel, AIAA 35th Aerospace Sciences Meeting and Exhibit (1997), AIAA Paper-1997-0236.
[14] H.-Y. Shih, Flame spread and interactions in an array of thin solids in low-speed concurrent flows, Combust. Theor. Model. 13 (2009) 443-459.
[15] H-Y. Shih, H.-C. Wu, An experimental study of upward flame spread and interactions over multiple solid fuels, J. Fire Sci. 26 (2008) 435-453.
[16] Y.-T. Tseng, J.S. T'ien, Limiting length, steady spread and non-growing flames in concurrent flow over solids, J. Heat Transf. 132 (2010) 091201-1.
[17] C. Li, Y.-T. Liao, J.S. T'ien, D.L. Urban, P. Ferkul, S. Olson, G.A. Ruff, J. Easton, Transient flame growth and spread processes over a large solid fabric in concurrent low-speed flows in microgravity –Model versus experiment, Proc. Combust. Inst. 37 (2019) 4163–4171.
[18] C. Li, Y.-T.T. Liao, Effects of ambient conditions on concurrent-flow flame spread over a wide thin solid in microgravity, Proc. Combust. Inst. 38 (2021) 4775-4784.
[19] Y. Li, Y.-T. Liao, P. Ferkul, Numerical Study of the Effects of Confinement on Concurrent-Flow Flame Spread in Microgravity, ASME J. Heat Transf. 142 (2020) 111301.
[20] Y. Li, Y.-T. Liao, P. Ferkul, M. Johnston, C. Bunnell, Effects of Confinement on Flame Spread in Microgravity, 49th International Conference on Environmental Systems (2020), ICES-2020-407.
[21] Y. Li, Y.-T. Liao, P. Ferkul, M.C. Johnston, C. Bunnell, Experimental study of concurrent-flow flame spread over thin solids in confined space in microgravity, Combust. Flame 227 (2021) 39–51.
[22] Y. Li, Y.-T.T. Liao, Numerical study of flame spread in a narrow flow duct in microgravity–effects of flow confinement and radiation reflection, Combust. Flame 235 (2022) 111714.
[23] L.K. Honda, P.D. Ronney, Mechanisms of concurrent-flow flame spread over solid fuel beds, Proc. Combust. Inst. 28 (2000) 2793-2801.
[24] M. Thomsen, C. Fernandez-Pello, D.L. Urban, G.A. Ruff, S.L. Olson, On simulating concurrent flame spread in reduced gravity by reducing ambient pressure, Proc. Combust. Inst. 37 (2019) 3793-3800.
[25] J. Kleinhenz, I.I. Feier, S.-Y. Hsu, J.S. T'ien, P.V. Ferkul, K.R. Sacksteder, Pressure modeling of upward flame spread and burning rates over solids in partial gravity, Combust. Flame 154(4) (2008) 637-643.
[26] M.J. Gollner, C.H. Miller, W. Tang, A.V. Singh, The effect of flow and geometry on concurrent flame spread, Fire Safety J. 91 (2017) 68-78.
[27] S.L. Olson, S.A. Gokoglu, D.L. Urban, G.A. Ruff, P.V. Ferkul, Upward flame spread in large enclosures: Flame growth and pressure rise, Proc. Combust. Inst. 35 (2015) 2623-2630.
[28] M. Thomsen, C. Fernandez-Pello, D. Urban, G. Ruff, S. Olson, Upward flame spread over a thin composite fabric: the effect of pressure and microgravity, 48th International Conference on Environmental Systems (2018), ICES-2018-231.
[29] L. Zhao, J. Fang, S. Tao, J. Wang, Y. Zhang, Effects of Ambient Parameters and Sample Width on Upward Flame Spread over Thermally Thin Solids, Fire Technol. 57 (2021) 145-161.
[30] X. Zhao, Y.-T.T. Liao, M.C. Johnston, J.S. T'ien, P.V. Ferkul, S.L. Olson, Concurrent flame growth, spread, and quenching over composite fabric samples in low speed purely forced flow in microgravity, Proc. Combust. Inst. 36 (2017) 2971-2978.

[31]C. Li, Y.-T.T. Liao, Numerical investigation of flame splitting phenomenon in upward flame spread over solids with a two-stage pyrolysis model, Combust. Sci. Technol. 190 (2018) 2082-2096.
[32]R.H. White, M.A. Dietenberger, Wood products: thermal degradation and fire, Encyclopedia of Materials: Science and Technology, Elsevier New York, USA, 2001, 9712–9716.
[33]J. Vleggaar, Laminar boundary-layer behaviour on continuous, accelerating surfaces," Chem. Eng. Sci. 32 (1977) 1517-1525. https://doi.org/10.1016/0009-2509(77)80249-2